Laser Chem. 1988, Vol. 8, pp. 61–78
Photocopying permitted by license only

Reprints available directly from the Publisher
Printed in the United Kingdom

High Resolution Spectroscopy of CF_3Br by Diode Laser in the Frequency Range 1070–1090 cm^{-1}

R. DE BEKKER, M. EBBEN, M. SNELS† and S. STOLTE

Fysisch Laboratorium, Katholieke Universiteit, Toernooiveld, 6525 ED Nijmegen, The Netherlands

(Received 21 May, 1987; in final form 4 October, 1987)

The IR absorption spectra of gaseous CF_3Br expanded in a molecular jet have been recorded with a linewidth of about 0.002 cm^{-1}. The rotational K-structure of the ν_1 fundamental has been resolved and the molecular constants ΔB and ΔA have been determined with an accuracy better than 5×10^{-6} cm^{-1}. Spectral features belonging to the ν_6- and ν_3-hotbands have been identified. For $CF_3{}^{79}Br$ ($CF_3{}^{81}Br$) improved values of the vibrational origins for the fundamental ν_1 = 1084.768(2) cm^{-1} (1084.520(2) cm^{-1}) and for its hotbands $\nu_3 + \nu_1 \leftarrow \nu_3$ = 1081.709(80) cm^{-1} (1081.065(40) cm^{-1}) and $\nu_6 + \nu_1 \leftarrow \nu_6$ = 1083.533(4) cm^{-1} (1083.288(4) cm^{-1}) have been determined.

KEY WORDS: Spectroscopy, CF_3Br, diode laser, molecular constants, hot bands.

INTRODUCTION

At several laboratories the IR absorption spectrum of CF_3Br has been studied extensively.[1–7] In the spectral region 1070–1100 cm^{-1}, Burczyk *et al.*,[1] using a Fourier Transform Spectrometer with a resolution of 0.015 cm^{-1}, observed individual rotational J-transitions of the ν_1-

† Present address: Laboratorio di Spettroscopia Moleculare, ENEA Centro di Frascati, CP 65, 1-00044 Frascati.

fundamental. However, the K-structure of this spectrum remained unresolved and in order to extract values for the rotational constants $\Delta A \equiv A' - A''$ and $\Delta B \equiv B' - B''$ bandcontour simulations had to be carried out. In the same work[1] hotband spectra exciting the ν_1 in thermally populated ν_6 and $2\nu_6$ vibrational levels have been observed, too. Hotbands due to ν_3- or ν_5-vibration, expected to possess comparable intensities to that of the $2\nu_6$ hotband, could not be identified.

In the present work the IR absorption spectrum of CF_3Br expanded in a supersonic jet, is recorded around 1085 cm^{-1}, using a tunable diode laser spectrometer. Due to the strong rotational cooling in the jet ($T_{rot} = 70K$) the number of absorption lines is reduced, which simplifies the spectra enormously. The vibrational cooling however, is much less efficient and, as will be shown in this paper, hotband structures are often intense enough to be observed. The line-width in this experiment is mainly determined by the divergency of the jet and is in our case about 70 MHz (0.0023 cm^{-1}).

In a similar study Davies and Morton-Jones[7a–7c] investigated the ν_1 band ($\simeq$ 1108 cm^{-1}) of CF_3Cl, using an expansion of 15% CF_3Cl in Ar. Of course the rotational cooling in a seeded expansion is even better ($T_{rot} \simeq 30K$) but the slightly better vibrational cooling will render the hotbands less intense, and the overall absorption intensity of the spectrum will be much weaker since there are less absorbing molecules in the jet. Moreover, by seeding freons like CF_3Br, CF_3Cl and others in a He or Ar beam, the average velocity will increase and consequently also the Doppler width of the absorption lines.

In order to combine a high sensitivity with narrow absorption lines a pure CF_3Br expansion was preferred to a seeded beam. The search for the hotbands was conducted in the low J part of the ν_1 fundamental, where its K-structure, due to its practical absence ($K \leq J$!), cannot obscure possible hotband lines. Supporting the findings of Burczyk *et al.*,[1] several spectral features belonging to the ν_6 hotband have been identified. Unfortunately the overlap between transitions originating from the ^{79}Br and the ^{81}Br isotopes in this region prevented us to identify the individual K-lines of the hotband. The remaining spectral features could be assigned as ν_3 hotband transitions.

By comparing the absorption strengths of assigned spectral transitions, a rotational (T_{rot}) and two vibrational temperatures (T_3 and T_6 indicating the populations of the ν_3- and ν_6-levels) for the probed molecules in the jet have been determined.

EXPERIMENTAL

A PbSnTe diode laser (Laser Analytics, model SP 5615-1060), mounted on the cold tip of a closed cycle cryogenic refrigerator (Air Products CSW 202), produced the radiation for the spectrometer, which is shown schematically in Figure 1. The laser was operated typically at 60 K and 400 mA, providing a single mode power of about 100 μW around 1085 cm^{-1}. As usual, the single mode radiation was obtained by filtering the multimode laser output through a grating monochromator. For this purpose the laser source was imaged onto the entrance slit (125 μm wide) of a Jarell Ash 82-415 monochromator (resolution 1 cm^{-1}), transmitting through an output slit 125 μm wide. For a typically continuous laserscan the frequency range of about 0.7 cm^{-1} taken at a fixed setting of the monochromator has always been

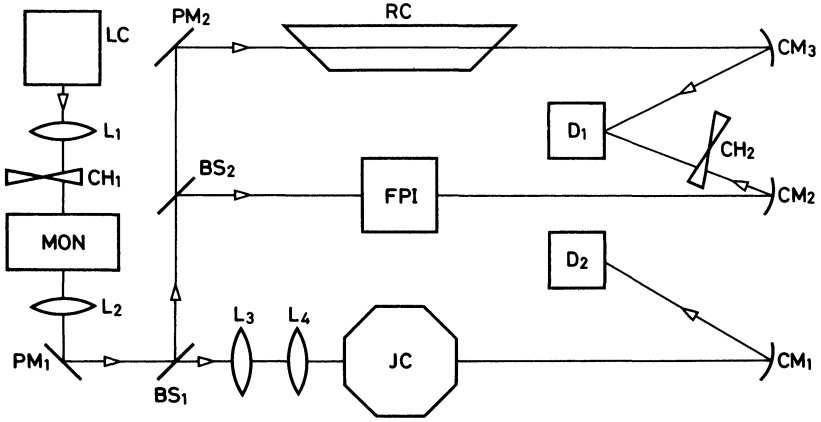

Figure 1 Diagram showing the experimental arrangement: the following abbreviations have been used: LC: diode laser on cryohead. L_1: ZnSe-lens (f = 1 inch) focusing the laser onto the entrance slit of the monochromator (MON). CH_1: mechanical chopper 200 Hz. L_2: ZnSe-lens (f = 9 sm) narrowing the laser into a practically parallel beam (Ø4 mm). PM_2, PM_3: flat goldcoated mirrors. BS_1, BS_2: beamsplitters made of NaCl, ZnSe respectively. RC: reference cell filled with SO_2. FPI: flat Fabry Perot etalon. L_3, L_4: (f = 19 cm, f = 1 inch) set of beam-narrowing lenses. JC: vacuum cell containing molecular jet. $CM_{1,2,3}$: concave mirrors (gold coated) imaging the laser beam onto the HgCdTe-detectors, D_1 and D_2. CH_2: chopper 800 Hz.

found to be smaller than the minimal mode spacing of emitted radiation by the diode laser. During such a scan, taking about an hour, the continuous frequency tuning has been achieved by changing the current through the diode laser at a fixed rate of 10^{-4} Amp/s. Our collection of spectral lines is the result of combining several scans. To permit lock-in detection the laser beam has been chopped mechanically at 200 Hz (by CH_1 of Figure 1) before entering the monochromator.

For a relative calibration of the laser frequency and to check the absence of mode hops, a small part of the main laser beam (through beamsplitters BS_1 and BS_2 of Figure 1) has been passed through a flat Ge crystal etalon (FSR. = 0.05 cm^{-1}) with a thickness of 1 inch. Another mechanical chopper operating at 800 Hz modulates this splitted part of the beam to allow its registration by one (D_1 in Figure 1) of our two HgCdTe semiconductor detectors (HCT 100 of Infrared Assoc. Inc.) operating at liquid nitrogen temperature.

The frequency of the laser beam has been estimated roughly by the setting of the mode filtering monochromator. Its precise value has been obtained by calibration on a SO_2 reference absorption spectrum, for which an accurate compilation[8] exists and which has been recorded simultaneously during the scan (see Figure 1). This has been done by passing a part of the main beam (by using beamsplitter BS_1 through an absorption cell (65 cm long) containing 10 mbar of SO_2. The two signals arriving at detector D_1 (see Figure 1) are disentangled by two lock-in amplifiers tuned to 200 Hz and 800 Hz, respectively.

Before being detected by the other HgCdTe detector (D_2 see Figure 1), the main part of the laser beam has been crossed perpendicularly with a molecular jet of pure CF_3Br. The path length for absorption of the laser beam through the jet has been increased by the insertion of a multiple pass (15×) system consisting of a pair of gold coated flat mirrors positioned 3 cm apart from each other (see Figure 2). At this probing region located in a plane 1 cm downstream from the nozzle opening, the laser beam has been narrowed to a diameter of about 0.5 mm Ø. The molecular jet has been expanded with a stagnation pressure of 1.5 bar through a 250 μm diameter nozzle at room temperature into a vacuum chamber pumped by a mechanical roots pump (500 m^3/h). CF_3Br gas of research purity (99.0% Matheson), containing Br isotopes in natural abundance (50.5% ^{79}Br and 49.5% ^{81}Br), was used without purification.

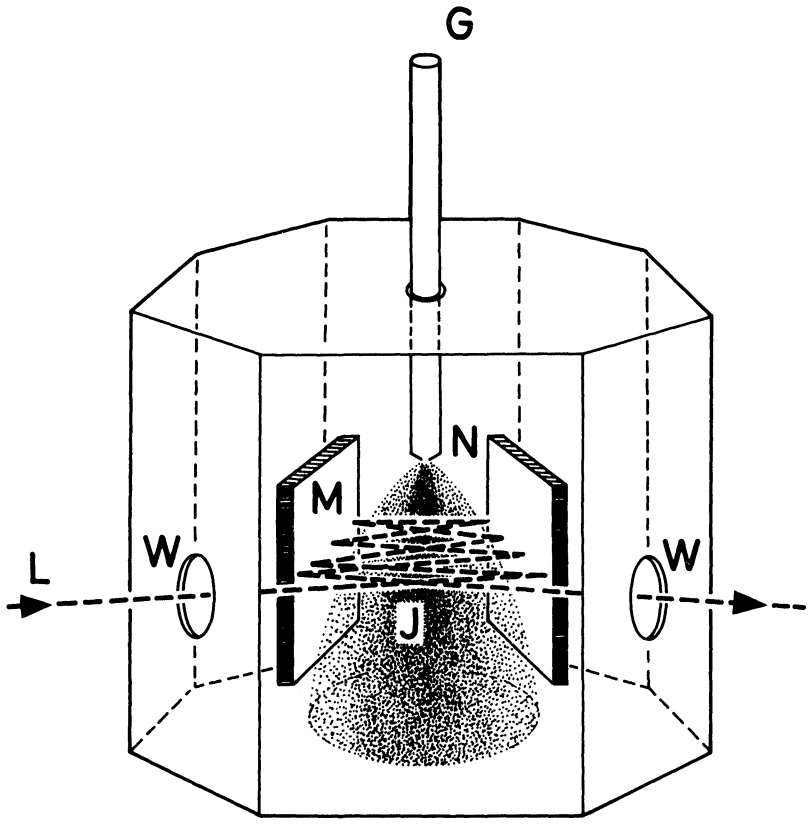

Figure 2 Multi pass arrangement for diode laser beam. The laser beam L is entering and leaving the vacuum cell through the double AR-coated ZnSe windows indicated with W. The CF_3Br gas, G, is expanded through nozzle N to form jet J which is dumped into a roots pump (not shown). The mirrors M are slightly tilted in respect to each other to provide a multi-pass for the laser beam shown as a dotted trajectory.

RESULTS AND DISCUSSION

In absence of Coriolis perturbations the rotational energy of a symmetric top molecule can be expressed in a simple Dunham series:[2,9]

$$E(J, K) = BJ(J + 1) + (A - B)K^2 - D_{JK}J(J + 1)K^2 - D_K K^4 - D_J J^2(J + 1)^2 + \ldots \quad (1)$$

Restricting to the explicit terms of Eq. (1), the transition frequency of

a rovibrational transition ($\Delta K = 0$) at which the vibrational angular momentum remains unchanged, for a $J - 1 \leftarrow J$ transition is found to be

$$\nu_P(J, K) = \nu_0 - 2JB'' + (J(J-1) - K^2)\,\Delta B + K^2\,\Delta A + 2JK^2 D''_{JK} - J(J-1)K^2\,\Delta D_{JK} + 4J^3 D''_J - J^2(J-1)^2\,\Delta D_J - \Delta D_K K^4 \quad (2)$$

for a $J \leftarrow J$ transition to be

$$\nu_Q(J, K) = \nu_0 + (J(J+1) - K^2)\,\Delta B + K^2\,\Delta A - J(J+1)K^2\,\Delta D_{JK} - J^2(J+1)^2\,\Delta D_J - \Delta D_K K^4 \quad (3)$$

and for a $J + 1 \leftarrow J$ transition to be

$$\nu_R(J, K) = \nu_0 + 2(J+1)B'' + ((J+2)(J+1) - K^2)\,\Delta B + K^2\,\Delta A - 2(J+1)K^2 D''_{JK} - ((J+2)(J+1)K^2\,\Delta D_{JK} - (J+1)^2(2J+3)D''_J - (J+1)^2(J+2)^2\,\Delta D_J - \Delta D_K K^4 \quad (4)$$

Here ν_1 equals the frequency of the band origin, $\Delta D_J \equiv D'_J - D''_J$ and $\Delta D_{JK} \equiv D'_{JK} - D''_{JK}$. The estimated values[7,10] for ν_1-vibrational transition D''_J (10^{-8} cm^{-1}), D''_{JK} (4×10^{-8} cm^{-1}), ΔD_J (2×10^{-9} cm^{-1}) and ΔD_{JK} (2×10^{-9} cm^{-1}) turn out to be so small that even for $J = 25$ and $K = 25$ the frequency shift due to these distortion terms remains smaller than 0.001 cm^{-1}. As, found also by[7a–7c], the frequency shifts induced by by the distortion terms, remain far too small to extract from the spectrum values for D''_J, D''_{JK}, ΔD_J or ΔD_{JK}. Thus, the dropping of these higher order contributions leads to the simpler expressions:

$$\nu_P(J, K) = \nu_0 - 2JB'' + (J(J-1) - K^2)\,\Delta B + K^2\,\Delta A \quad (5)$$

$$\nu_Q(J, K) = \nu_0 + (J(J+1) - K^2)\,\Delta B + K^2\,\Delta A \quad (6)$$

$$\nu_R(J, K) = \nu_0 + 2(J+1)B'' + ((J+2)(J+1) - K^2)\,\Delta B + K^2\,\Delta A \quad (7)$$

which we have used to analyse the experimental data.

As a first target of investigation the spectral region of the *P*-branches of high *J*-levels (1081.1 – 1082.6 cm^{-1}) of the fundamental ν_1-absorption has been chosen. Here the congestion induced by overlapping *K*-structures of the $CF_3{}^{79}Br$ and $CF_3{}^{81}Br$ isotopomers remains minimal since, as is shown in Figure 3, subsequent transitions of the

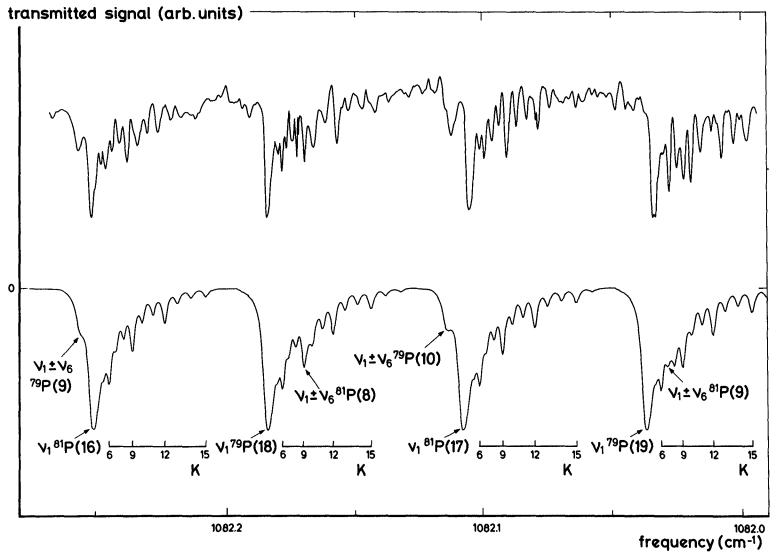

Figure 3 Infrared absorption spectrum of CF_3Br in a jet at the *P*-branch region between 1082.0–1082.3 cm^{-1}. The upper trace displays the recorded diode laser signal (vertical scale) as a function of laser frequency (horizontal scale). The latter was obtained by interpolation between calibrating SO_2-transitions (see text). The 0-mark at the vertical scale corresponds with the situation of switched off laser beam and indicates also the lower trace representing the simulated spectrum. The lower horizontal frequency axis coincides with the situation of a fully absorbed laser beam of the simulation. The various transitions have been identified and also labelled according to the participating isotopomer with a superscript indicating the mass of the associated Br-atom. *K*-ladders designate the *K*-transitions resolved (see Table I). Hotband transitions, e.g. $\nu_1 + \nu_6 \leftarrow \nu_6$ have been designated in short hand notation, $\nu_1 \pm \nu_6$. The resemblance of the measured and simulated spectra turned out to be optimal after inserting a Lorentzian linewidth $\Delta\nu = 0.0023\ cm^{-1}$ (fwhm) and a value of $a = 1.2$ for the constant simulating the optical density integrated along the absorption path.

^{79}Br-isotope occur nearly halfway between those of the ^{81}Br-isotope. Although contributions of ν_6-hotbands are expected in this region, the vibrational cooling induced by the expansion[11] and the fact that the optimally populated *J*-level occur at about $J \simeq 30$ render the hotband contributions much weaker. Finally, since the rotational constants of the excited vibrational states are smaller than those of the ground level, for *P*-branch type of transitions one has to do with a dispersion, and not with a piling-up of spectral features (due to the onset of band head formations). As shown in Figure 3 (between 1082.0–1082.3 cm^{-1})

individual K-transitions (from $K = 5$ on) have been resolved and can easily be identified. This assignment has been verified by checking the predominance of the statistical weight of (2:1) of the para levels ($K = 0, 3, 6, 9, \ldots$) in comparison to the ortho levels ($K = 1, 2, 4, 5, \ldots$). The $K = 0, 1, 2, 3$ transitions were not resolvable and they have been recorded as contributions to one peak, whose maximum corresponds to the center of $K = 2$ transition. In Table I the frequencies of resolved K-peaks ($K \geq 5$) from the $J = 17$–24 ($CF_3{}^{79}Br$) and from $J = 14$–23 ($CF_3{}^{81}Br$) have been collected.

These frequencies listed have been determined by interpolating the simultaneously recorded SO_2-reference spectrum (linewidth 6.5×10^{-3} cm^{-1}) as a third order polynomial in the diode current (which has been linearly varied during the recording time) for a single continuous scan. Such a polynomial turns out to contain enough parameters[12] to reproduce the frequencies[8] of all reference lines contained in a single scan (5–10) within their accuracy. The assignment of J values for the individual J, K transitions has been taken according to the lower resolution work of Burczyk *et al.*[1] After insertion of the accurately determined rotational constant B'' by Sheridan and Gordon[10] in Eq. (5), a least square fit to the measured line position of Table 1 has yielded new values for the difference in rotational constants of the ν_1-excited and ground vibrational states ΔA, ΔB as well as an

Table I Observed values of J, K-resolved ν_1 transitions compared with calculated values obtained from fit. All frequencies are given in (cm^{-1}).

	Transition	Observed	Calculated	obs–calc
79	$J = 15 \rightarrow 14$ $K = 6$	1082.616	1082.618	−0.002
79	$J = 15 \rightarrow 14$ $K = 7$	1082.614	1082.616	−0.002
79	$J = 15 \rightarrow 14$ $K = 8$	1082.611	1082.613	−0.002
79	$J = 15 \rightarrow 14$ $K = 9$	1082.608	1082.610	−0.002
79	$J = 15 \rightarrow 14$ $K = 10$	1082.605	1082.607	−0.002
79	$J = 17 \rightarrow 16$ $K = 5$	1082.328	1082.328	<0.001
79	$J = 17 \rightarrow 16$ $K = 6$	1082.326	1082.326	<0.001
79	$J = 17 \rightarrow 16$ $K = 7$	1082.323	1082.323	<0.001
79	$J = 17 \rightarrow 16$ $K = 8$	1082.321	1082.320	0.001
79	$J = 17 \rightarrow 16$ $K = 9$	1082.318	1082.317	0.001
79	$J = 17 \rightarrow 16$ $K = 10$	1082.314	1082.314	<0.001
79	$J = 17 \rightarrow 16$ $K = 11$	1082.310	1082.310	<0.001
79	$J = 17 \rightarrow 16$ $K = 12$	1082.306	1082.306	<0.001
79	$J = 17 \rightarrow 16$ $K = 13$	1082.301	1082.301	<0.001
79	$J = 17 \rightarrow 16$ $K = 14$	1082.295	1082.296	−0.001

Table I *continued.*

	Transition	Observed	Calculated	obs–calc
79	$J = 18 \rightarrow 17$ $K = 5$	1082.181	1082.181	<0.001
79	$J = 18 \rightarrow 17$ $K = 6$	1082.179	1082.179	<0.001
79	$J = 18 \rightarrow 17$ $K = 7$	1082.177	1082.176	0.001
79	$J = 18 \rightarrow 17$ $K = 8$	1082.175	1082.173	0.002
79	$J = 18 \rightarrow 17$ $K = 9$	1082.173	1082.170	0.003
79	$J = 18 \rightarrow 17$ $K = 10$	1082.170	1082.167	0.003
79	$J = 18 \rightarrow 17$ $K = 11$	1082.167	1082.163	0.004
79	$J = 18 \rightarrow 17$ $K = 12$	1082.162	1082.159	0.003
79	$J = 18 \rightarrow 17$ $K = 13$	1082.157	1082.154	0.003
79	$J = 18 \rightarrow 17$ $K = 14$	1082.153	1082.149	0.004
79	$J = 19 \rightarrow 18$ $K = 6$	1082.028	1082.031	−0.003
79	$J = 19 \rightarrow 18$ $K = 7$	1082.025	1082.029	−0.004
79	$J = 19 \rightarrow 18$ $K = 8$	1082.023	1082.026	−0.003
79	$J = 19 \rightarrow 18$ $K = 9$	1082.020	1082.023	−0.003
79	$J = 19 \rightarrow 18$ $K = 10$	1082.016	1082.019	−0.003
79	$J = 19 \rightarrow 18$ $K = 11$	1082.012	1082.016	−0.004
79	$J = 19 \rightarrow 18$ $K = 12$	1082.008	1082.011	−0.003
79	$J = 19 \rightarrow 18$ $K = 13$	1082.003	1082.007	−0.004
79	$J = 19 \rightarrow 18$ $K = 14$	1081.999	1082.002	−0.003
79	$J = 19 \rightarrow 18$ $K = 15$	1081.993	1081.997	−0.004
79	$J = 19 \rightarrow 18$ $K = 16$	1081.988	1081.991	−0.003
79	$J = 20 \rightarrow 19$ $K = 5$	1081.888	1081.885	0.003
79	$J = 20 \rightarrow 19$ $K = 6$	1081.885	1081.883	0.002
79	$J = 20 \rightarrow 19$ $K = 7$	1081.883	1081.881	0.002
79	$J = 20 \rightarrow 19$ $K = 8$	1081.881	1081.878	0.003
79	$J = 20 \rightarrow 19$ $K = 9$	1081.878	1081.875	0.003
79	$J = 20 \rightarrow 19$ $K = 10$	1981.874	1081.872	0.002
79	$J = 20 \rightarrow 19$ $K = 11$	1981.871	1081.868	0.003
79	$J = 20 \rightarrow 19$ $K = 12$	1081.867	1081.863	0.004
79	$J = 20 \rightarrow 19$ $K = 13$	1081.862	1981.859	0.003
79	$J = 20 \rightarrow 19$ $K = 14$	1081.858	1081.854	0.004
79	$J = 20 \rightarrow 19$ $K = 15$	1081.853	1081.849	0.004
79	$J = 21 \rightarrow 20$ $K = 6$	1081.736	1081.735	0.001
79	$J = 21 \rightarrow 20$ $K = 9$	1081.727	1081.727	<0.001
79	$J = 21 \rightarrow 20$ $K = 10$	1081.723	1081.723	<0.001
79	$J = 21 \rightarrow 20$ $K = 11$	1081.720	1081.719	0.001
79	$J = 21 \rightarrow 20$ $K = 12$	1081.715	1081.715	<0.001
79	$J = 21 \rightarrow 20$ $K = 13$	1081.711	1081.711	<0.001
79	$J = 21 \rightarrow 20$ $K = 14$	1081.706	1081.706	<0.001
79	$J = 21 \rightarrow 20$ $K = 15$	1081.700	1081.700	<0.001
79	$J = 22 \rightarrow 21$ $K = 6$	1081.588	1081.586	0.002
79	$J = 22 \rightarrow 21$ $K = 9$	1081.580	1081.578	0.002
79	$J = 22 \rightarrow 21$ $K = 10$	1081.576	1081.575	0.001
79	$J = 22 \rightarrow 21$ $K = 11$	1081.572	1081.571	0.001
79	$J = 22 \rightarrow 21$ $K = 12$	1081.567	1081.567	<0.001
79	$J = 22 \rightarrow 21$ $K = 13$	1081.563	1081.562	0.001
79	$J = 22 \rightarrow 21$ $K = 14$	1081.558	1081.557	0.001
79	$J = 22 \rightarrow 21$ $K = 15$	1081.552	1081.552	<0.001

Table I *continued.*

	Transition	Observed	Calculated	obs–calc
79	$J = 23 \rightarrow 22$ $K = 6$	1081.437	1081.437	<0.001
79	$J = 23 \rightarrow 22$ $K = 7$	1081.435	1081.435	<0.001
79	$J = 23 \rightarrow 22$ $K = 8$	1081.432	1081.432	<0.001
79	$J = 23 \rightarrow 22$ $K = 9$	1081.429	1081.429	<0.001
79	$J = 23 \rightarrow 22$ $K = 10$	1081.425	1081.425	<0.001
79	$J = 23 \rightarrow 22$ $K = 11$	1081.420	1081.422	−0.002
79	$J = 23 \rightarrow 22$ $K = 12$	1081.416	1081.417	−0.001
79	$J = 23 \rightarrow 22$ $K = 13$	1081.412	1081.413	−0.001
79	$J = 23 \rightarrow 22$ $K = 14$	1081.407	1081.408	−0.001
79	$J = 23 \rightarrow 22$ $K = 15$	1081.401	1081.403	−0.002
79	$J = 24 \rightarrow 23$ $K = 6$	1081.287	1081.288	−0.001
79	$J = 24 \rightarrow 23$ $K = 9$	1081.279	1081.279	<0.001
79	$J = 24 \rightarrow 23$ $K = 10$	1081.275	1081.276	−0.001
79	$J = 24 \rightarrow 23$ $K = 11$	1081.271	1081.272	−0.001
79	$J = 24 \rightarrow 23$ $K = 12$	1081.267	1081.268	−0.001
79	$J = 24 \rightarrow 23$ $K = 13$	1081.262	1081.263	−0.001
79	$J = 24 \rightarrow 23$ $K = 14$	1081.257	1081.258	−0.001
79	$J = 24 \rightarrow 23$ $K = 15$	1081.252	1081.253	−0.001
81	$J = 14 \rightarrow 13$ $K = 6$	1082.536	1082.536	<0.001
81	$J = 14 \rightarrow 13$ $K = 7$	1082.534	1082.533	0.001
81	$J = 14 \rightarrow 13$ $K = 8$	1082.531	1082.531	<0.001
81	$J = 14 \rightarrow 13$ $K = 9$	1082.528	1082.527	0.001
81	$J = 14 \rightarrow 13$ $K = 10$	1082.524	1082.524	<0.001
81	$J = 14 \rightarrow 13$ $K = 11$	1082.521	1082.520	0.001
81	$J = 14 \rightarrow 13$ $K = 12$	1082.517	1082.516	0.001
81	$J = 15 \rightarrow 14$ $K = 6$	1082.394	1082.392	0.002
81	$J = 15 \rightarrow 14$ $K = 7$	1082.391	1082.389	0.002
81	$J = 15 \rightarrow 14$ $K = 8$	1082.388	1082.386	0.002
81	$J = 15 \rightarrow 14$ $K = 9$	1082.385	1082.383	0.002
81	$J = 15 \rightarrow 14$ $K = 10$	1082.381	1082.380	0.001
81	$J = 15 \rightarrow 14$ $K = 11$	1082.377	1082.376	0.001
81	$J = 15 \rightarrow 14$ $K = 12$	1082.372	1082.371	0.001
81	$J = 16 \rightarrow 15$ $K = 5$	1082.249	1082.249	<0.001
81	$J = 16 \rightarrow 15$ $K = 6$	1082.248	1082.247	0.001
81	$J = 16 \rightarrow 15$ $K = 7$	1082.245	1082.244	0.001
81	$J = 16 \rightarrow 15$ $K = 8$	1082.242	1082.242	<0.001
81	$J = 16 \rightarrow 15$ $K = 9$	1082.239	1082.238	0.001
81	$J = 16 \rightarrow 15$ $K = 10$	1082.235	1082.235	<0.001
81	$J = 16 \rightarrow 15$ $K = 11$	1082.231	1082.231	<0.001
81	$J = 16 \rightarrow 15$ $K = 12$	1082.227	1082.227	<0.001
81	$J = 16 \rightarrow 15$ $K = 13$	1082.222	1082.222	<0.001
81	$J = 17 \rightarrow 16$ $K = 5$	1082.102	1082.104	−0.002
81	$J = 17 \rightarrow 16$ $K = 6$	1082.100	1082.102	−0.002
81	$J = 17 \rightarrow 16$ $K = 7$	1082.097	1082.099	−0.002
81	$J = 17 \rightarrow 16$ $K = 8$	1082.094	1082.096	−0.002
81	$J = 17 \rightarrow 16$ $K = 9$	1082.091	1082.093	−0.002
81	$J = 17 \rightarrow 16$ $K = 10$	1082.087	1082.090	−0.003

Table I *continued.*

	Transition	Observed	Calculated	obs–calc
81	$J = 17 \rightarrow 16$ $K = 11$	1082.083	1082.086	−0.003
81	$J = 17 \rightarrow 16$ $K = 12$	1082.079	1082.082	−0.003
81	$J = 17 \rightarrow 16$ $K = 13$	1082.074	1082.077	−0.003
81	$J = 18 \rightarrow 17$ $K = 6$	1081.955	1081.956	−0.001
81	$J = 18 \rightarrow 17$ $K = 7$	1081.952	1081.954	−0.002
81	$J = 18 \rightarrow 17$ $K = 8$	1081.950	1081.951	−0.001
81	$J = 18 \rightarrow 17$ $K = 9$	1081.946	1081.948	−0.002
81	$J = 18 \rightarrow 17$ $K = 10$	1081.942	1081.944	−0.002
81	$J = 18 \rightarrow 17$ $K = 11$	1081.939	1081.940	−0.001
81	$J = 18 \rightarrow 17$ $K = 12$	1081.935	1081.936	−0.001
81	$J = 18 \rightarrow 17$ $K = 13$	1081.931	1081.931	<0.001
81	$J = 19 \rightarrow 18$ $K = 6$	1081.812	1081.810	0.002
81	$J = 19 \rightarrow 18$ $K = 9$	1081.803	1081.802	0.001
81	$J = 19 \rightarrow 18$ $K = 10$	1081.800	1081.798	0.002
81	$J = 19 \rightarrow 18$ $K = 11$	1081.796	1081.794	0.002
81	$J = 19 \rightarrow 18$ $K = 12$	1081.791	1081.790	0.001
81	$J = 19 \rightarrow 18$ $K = 13$	1081.786	1081.785	0.001
81	$J = 19 \rightarrow 18$ $K = 14$	1081.781	1081.780	0.001
81	$J = 19 \rightarrow 18$ $K = 15$	1081.776	1081.775	0.001
81	$J = 20 \rightarrow 19$ $K = 6$	1081.664	1081.664	<0.001
81	$J = 20 \rightarrow 19$ $K = 9$	1081.656	1081.655	0.001
81	$J = 20 \rightarrow 19$ $K = 10$	1081.652	1081.652	<0.001
81	$J = 20 \rightarrow 19$ $K = 11$	1081.648	1081.648	<0.001
81	$J = 20 \rightarrow 19$ $K = 12$	1081.644	1081.644	<0.001
81	$J = 20 \rightarrow 19$ $K = 13$	1081.639	1081.639	<0.001
81	$J = 20 \rightarrow 19$ $K = 15$	1081.629	1081.629	<0.001
81	$J = 21 \rightarrow 20$ $K = 6$	1081.519	1081.517	0.002
81	$J = 21 \rightarrow 20$ $K = 9$	1981.510	1081.509	0.001
81	$J = 21 \rightarrow 20$ $K = 10$	1081.506	1081.505	0.001
81	$J = 21 \rightarrow 20$ $K = 11$	1081.502	1081.501	0.001
81	$J = 21 \rightarrow 20$ $K = 12$	1081.498	1081.497	0.001
81	$J = 21 \rightarrow 20$ $K = 13$	1081.494	1081.492	0.002
81	$J = 21 \rightarrow 20$ $K = 14$	1081.488	1081.487	0.001
81	$J = 21 \rightarrow 20$ $K = 15$	1081.482	1081.482	<0.001
81	$J = 22 \rightarrow 21$ $K = 6$	1081.369	1081.370	−0.001
81	$J = 22 \rightarrow 21$ $K = 9$	1081.361	1081.362	−0.001
81	$J = 22 \rightarrow 21$ $K = 10$	1081.357	1081.358	−0.001
81	$J = 22 \rightarrow 21$ $K = 11$	1081.354	1081.354	<0.001
81	$J = 22 \rightarrow 21$ $K = 12$	1081.349	1081.350	−0.001
81	$J = 22 \rightarrow 21$ $K = 13$	1081.344	1081.345	−0.001
81	$J = 22 \rightarrow 21$ $K = 14$	1081.340	1081.340	<0.001
81	$J = 22 \rightarrow 21$ $K = 15$	1081.334	1081.335	−0.001
81	$J = 23 \rightarrow 22$ $K = 6$	1081.223	1081.222	0.001
81	$J = 23 \rightarrow 22$ $K = 9$	1981.214	1981.214	<0.001
81	$J = 23 \rightarrow 22$ $K = 12$	1081.203	1082.202	0.001
81	$J = 23 \rightarrow 22$ $K = 14$	1081.193	1081.193	<0.001
81	$J = 23 \rightarrow 22$ $K = 15$	1081.188	1081.187	0.001

improved value for the ν_1-fundamental. In Table II our results are compared with those determined previously.[1,7,10] The calculated line positions in Table I differ less than 0.004 cm^{-1} from the observed line positions. Apparently, the observation that the ν_1-vibration, besides a Fermi interaction with $2\nu_5$, is not affected by (local) perturbations can be extended to a level of about 10^{-3} cm^{-1}.

In the spectral region between 1084.5–1085.5 cm^{-1} several hotband transitions have been observed. The molecular constants and line positions obtained by Burczyk *et al.*[1] have made it possible to assign the observed spectral structures which resulted from $\nu_1 + \nu_6 \leftarrow \nu_6$ transitions and have been collected in Table III. Unfortunately, the overlap of *K*-structures of CF_3 ^{79}Br and CF_3 ^{81}Br, as shown in Figure 4, does not permit an identification of individual *K* hotband transitions. Assuming the additivity of rotational constants[1], i.e. $\Delta B = B_{\nu_1+\nu_6} - B_{\nu_6} = B_{\nu_1} - B_0$ and $\Delta A = A_{\nu_1+\nu_6} - A_{\nu_6} = A_{\nu_6} = A_{\nu_1} - A_0$, the values of Table II for ΔA and ΔB have been used as input parameters in Eq. (7) for the fit of the data collected in Table III. The agreement between all calculated and observed frequencies is again better than 0.004 cm^{-1}. The rovibrational constants obtained are listed in Table IV, and are found to be in agreement (but more accurate) with earlier work.[1,7,10]

Table II Molecular parameters of the ν_1-fundamental transition. The values denoted as (this work) are preferred because of their improved accuracy.

	CF_3 ^{79}Br[a]	CF_3 ^{81}Br[a]
ν_1	1084.763(2) [1]	1084.521(2) [1]
	1084.768(2)[b] (This work)	1084.520(2)[b] (This work)
B''	0.069984[c] [7,10]	0.069331[c] [7,10]
$\Delta B = B' - B''$	-212×10^{-6} [7]	
	$-218(31) \times 10^{-6}$ [1]	$-217(39) \times 10^{-6}$ [1]
	$-208(4) \times 10^{-6}$ (This work)	$-203(3) \times 10^{-6}$ (This work)
$\Delta A = A' - A''$	$-398(10) \times 10^{-6}$ [7]	
	$-440(40) \times 10^{-6}$ [1]	$-440(40) \times 10^{-6}$ [1]
	$-391(7) \times 10^{-6}$ (This work)	$-390(6) \times 10^{-6}$ (This work)

[a] All parameters in (cm^{-1}).

[b] The calibration lines have an estimated uncertainty of 0.004 cm^{-1}.[8] All individual measured transitions have been given this same uncertainty as an input for our fit. As in other work (e.g.[7a]) the undershoot of the statistical (1std) error of the band origin, listed in the table, compared to the fundamental and systematical uncertainty of calibration remains small enough to allow ignorance of the latter in the final result.

[c] Input value for fit found compatible with data of Table I.

Table III Observed values of *J*-resolved transitions $\nu_1 + \nu_6 \leftarrow \nu_6$ are compared with calculated values extracted from fit. All frequencies are given in cm^{-1}.

J	*K*	Transition	Calculated	Observed	cal–obs
9	2	R ^{79}Br	1084.903	1084.905	−0.002
10	2	R ^{79}Br	1085.038	1085.038	0.000
11	2	R ^{79}Br	1085.172	1085.173	−0.001
12	2	R ^{79}Br	1085.307	1085.306	0.001
13	2	R ^{79}Br	1085.440	1085.441	−0.001
16	2	R ^{79}Br	1085.839	1085.843	−0.004
17	2	R ^{79}Br	1085.971	1085.972	−0.001
18	2	R ^{79}Br	1086.103	1086.102	0.001
19	2	R ^{79}Br	1086.234	1086.235	−0.001
20	2	R ^{79}Br	1086.365	1086.365	0.000
21	2	R ^{79}Br	1086.496	1086.495	0.001
22	2	R ^{79}Br	1086.626	1086.623	0.003
10	2	R ^{81}Br	1084.781	1084.782	−0.001
11	2	R ^{81}Br	1084.914	1084.916	−0.002
13	2	R ^{81}Br	1085.180	1085.179	0.001
14	2	R ^{81}Br	1085.312	1085.311	0.001
18	2	R ^{81}Br	1085.837	1085.840	−0.003
19	2	R ^{81}Br	1085.967	1085.967	0.000
20	2	R ^{81}Br	1086.097	1086.095	0.002
21	2	R ^{81}Br	1086.227	1086.227	0.000
22	2	R ^{81}Br	1086.356	1086.355	0.001
23	2	R ^{81}Br	1086.484	1086.484	0.000

Table IV Molecular parameters of the $\nu_1 + \nu_6 \leftarrow \nu_6$ hotband transitions. The values denoted as (this work) agree with earlier work.

	$CF_3{}^{79}Br$[a]	$CF_3{}^{81}Br$[a]
$\nu_1 + \nu_6 \leftarrow \nu_6$	1083.530(1) [7]	
	1083.525(4) [1]	1083.284(2) [1]
	1083.533(4)[b] (This work)	1083.288(4)[b] (This work)
ΔB	-208×10^{-6} [c] (see Table II)	-203×10^{-6} [c] (see Table II)
ΔA	-391×10^{-6} [c] (see Table II)	-390×10^{-6} [c] (see Table II)
B_{ν_6}	0.069718(100) (This work)	0.069124(100) (This work)
$B_{\nu_6} - B_0$	-120×10^{-6} [7,10]	
	$-170(200) \times 10^{-6}$ [1]	$-150(200) \times 10^{-6}$ [1]
	$-266(100) \times 10^{-6}$ (This work)	$-207(100) \times 10^{-6}$ (This work)
X_{16}	−1.238(3) [1]	−1.237(3) [1]
	−1.235(5) (This work)	−1.232(5) (This work)

[a] All parameters in (cm^{-1}).

[b] Calibration lines have an estimated uncertainty of 0.004 cm^{-1}.[8] All individual measured transitions have been given this same uncertainty as an input for our fit.

[c] Input value for fit found compatible with data of Table III.

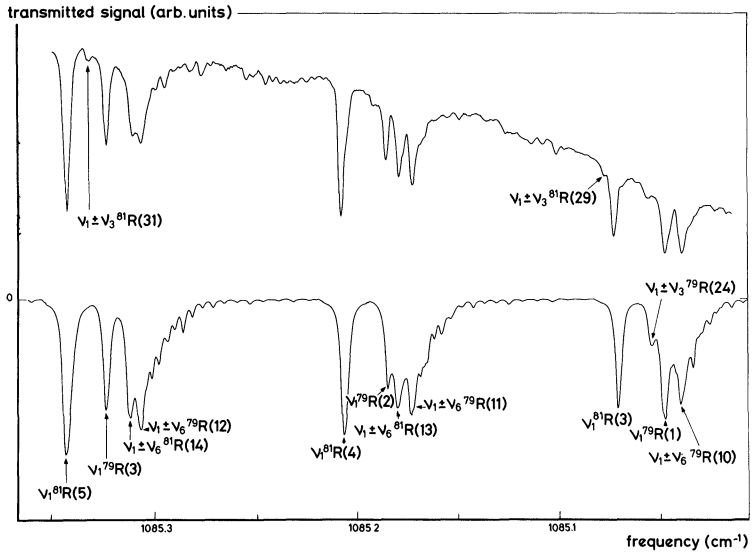

Figure 4 Infrared absorption spectrum of CF_3Br in a jet at the *R*-branch region between 1085.0–1085.3 cm^{-1}. During this scan the intensity of the diode laser degraded considerably at the range of lower laser frequency (see upper curve). The simulated intensity (as in Figure 3) assumes constant laser intensity. The interferences of neighbouring transitions of various isotopomers and hotbands make it impossible in this region to assign *K*-structures. For all other details see caption of Figure 3. The same value of a and $\Delta\nu$ have also been used here.

In the investigated region between 1084.5–1085.2 cm^{-1} spectral features of an until now never resolved hotband of ν_1 has been found and assigned as a $\nu_1 + \nu_3 \leftarrow \nu_3$ transition. The spectral transitions belonging to this hotband have been identified and are listed in Table V. Of course again the *K*-structure could not be resolved and as in preceding cases the maximum of absorption turns out to coincide also with the $K = 2$ component. Consequently the calculated values in Tables III and V all refer to the $K = 2$ component. Insertion of the ΔA and ΔB values, used previously for the $\nu_1 + \nu_6 \leftarrow \nu_6$ and ν_1 bands, in Eq. (7) resulted in accurate values for $\nu_1 + \nu_3 \leftarrow \nu_3$ and B_{ν_3} (see Table VI) which reproduced the experimental line frequencies (within 0.002 cm^{-1}, see Table V) quite satisfactory. In Table VI the resulting spectroscopic constants: $X_{13} = (\nu_1 + \nu_3 \leftarrow \nu_3) - \nu_3$ and $B_{\nu_3} - B_0$ have been found to agree with previous work.[5]

Table V Observed values of J-resolved transitions of $\nu_1 + \nu_3 \leftarrow \nu_3$ are compared with calculated values obtained from fit. All values given in cm^{-1}.

J	K	Transition	Calculated	Observed	cal–obs[f]
22	2	R ^{79}Br	1084.796	1084.796[a]	0.000
23	2	R ^{79}Br	1084.925	1084.926	−0.002
24	2	R ^{79}Br	1085.054	1085.054	0.000
25	2	R ^{79}Br	1085.183	1085.183[b]	0.000
26	2	R ^{79}Br	1085.311	1085.312[c]	−0.001
27	2	R ^{79}Br	1085.439	1085.440[d]	−0.001
27	2	R ^{81}Br	1084.821	1084.821	−0.000
28	2	R ^{81}Br	1084.951	1084.950	−0.001
29	2	R ^{81}Br	1085.077	1085.077	−0.000
30	2	R ^{81}Br	1085.203	[e]	
31	2	R ^{81}Br	1085.331	1085.332	−0.001

[a] Obscured by ν_1 $J = 1 \leftarrow 0$ ^{81}Br (1084.796 cm^{-1}).
[b] Obscured by ν_6 hotband $J = 14 \leftarrow 13$ ^{81}Br (1085.180 cm^{-1}).
[c] Obscured by ν_6 hotband $J = 15 \leftarrow 14$ ^{81}Br (1085.312 cm^{-1}).
[d] Obscured by ν_6 hotband $J = 16 \leftarrow 15$ ^{81}Br (1085.444 cm^{-1}) and by the ν_6 hotband $J = 14 \leftarrow 13$ ^{79}Br (1085.440 cm^{-1}).
[e] Obscured by ν_1 $J = 5 \leftarrow 4$ ^{81}Br (1085.206 cm^{-1}).
[f] The low number of unobscured lines made it necessary to include in the fit the lines a,b,c,d also. For the latter lines the accuracy of line frequency was degraded to ± 0.020 cm^{-1}

In order to check the consistency of the assignments, and to obtain information about the state distribution of probed molecules, a simulation of the observed absorption profiles (Figures 3 and 4) has been carried out. Usually partially thermal state distributions are expected to occur in molecular jets. To model the essentials of the state distribution of the CF_3Br molecules probed along the laserpath (see Figure 2), separate parameters for the vibrational (T_{vib}) and rotational (T_{rot}) temperatures have been invoked. The absorption strength of an individual rovibrational transition of a symmetric top is assumed to be proportional to:[8]

$$\alpha_{J,K,i} = A_{KJ} \times g_{KJ} \times \exp(-h\nu_i/kT_i) \times \exp(-E_{rot}/kT_{rot}) \qquad (8)$$

where A_{KJ} stands for the Hönl-London factor and g_{KJ} the statistical weight of the absorbing JK-level possessing a rotational energy, E_{rot}. The vibrational energy, $h\nu_i$ equals zero for the groundstate. To estimate T_{rot}, the absorption-strengths of different K-components within one J-transition have been compared. The relative strength of

Table VI Molecular parameters of the $\nu_1 + \nu_3 \leftarrow \nu_3$ hotband transitions. The values denoted as (this work) are found to agree with earlier results.

	$CF_3{}^{79}Br$[a]	$CF_3{}^{81}Br$[a]
$\nu_1 + \nu_3 \leftarrow \nu_3$	1081.709(80)[b] (This work)	1081.065(40)[b] (This work)
ΔB	-208×10^{-6} [c] (see Table II)	-203×10^{-6} [c] (see Table II)
ΔA	-391×10^{-6} [c] (see Table II)	-390×10^{-6} [c] (see Table II)
B_{ν_3}	0.06962(100) (This work)	0.06983(60) (This work)
$B_{\nu_3} - B_0$	-57×10^{-6} [d] [5]	
	$-36(100) \times 10^{-5}$ (This work)	$50(60) \times 10^{-5}$ (This work)[e]
X_{13}	$-3.086(20)$ [5]	$-3.37(5)$ [5]
	$-3.059(80)$ (This work)	$-3.55(40)$ (This work)

[a] All parameters in (cm^{-1}).

[b] Calibration lines have an estimated uncertainty of 0.004 cm^{-1}.[8] All individual transitions have been given this same uncertainty as an input for our fit.

[c] input value for fit found to be compatible with our data of Table V.

[d] Obtained by subtraction of the effective vibration–rotation interaction constants $\alpha_1^B - \alpha_{(\nu_1+\nu_3)}^B$ listed in Table VIII of [5].

[e] A negative value expected for this quantity is allowed with statitical uncertainty.

hot-band transitions with respect to nearby (closer than 0.1 cm^{-1}) ν_1-transitions have been compared to calculate T_{vib}. At the frequencies of strong lines (see Figures 3 and 4) we found the transmitted laser beam I to be much weaker than the full laser beam I_0, detected when the jet was switched off. To account for Beer's Law we employed the relation $I = I_0 \exp(-\alpha_{J,K,i} a)$, where the constant a, proportional to the optical density, has been adjusted empirically to simulate the measured spectrum.

This procedure yielded a rotational temperature of 70 ± 20 K, a vibrational temperature which reflects the population of the ν_6 level $T_6 = 220 \pm 20$ K and a T_3 reflecting the population of the ν_3 level of 190 ± 20 K. A simulation of the absorption spectrum assuming these vibrational temperatures, a rotational temperature of 70 K and a linewidth of 0.0023 cm^{-1}, is shown in Figure 3, together with the experimental spectrum. $T_{rot} = 70$ K of our pure expansion appears to be considerably higher than the $T_{rot} \simeq 30$ K, found for 15% CF_3Cl seeded in Ar[7a–7c] where no hotbands have been reported. Here we want to stress that the relatively simple appearance of the spectrum is a consequence of the application of the molecular jet technique. Assuming a thermal equilibrium in the expansion (the results show that this assumption is not completely true) one finds that for a vibrational

temperature of 200 K the relative absorption strength of the possible hot-bands with respect to the ν_1 vibration is 1000 : 4 : 82 : 40 : 230 : 40 (ν_1 : ν_2HB : ν_3HB : ν_5HB : ν_6HB : $2\nu_6$HB), where the intensity of the hot-bands (HB) of the ν_1 and ν_4 are even much smaller. More sensitive measurements will be necessary to reveal other hot-bands than those observed here.

Apart from the spectral data our measurements provide some information about the vibrational relaxation in molecular jet expansion. The possibly higher vibrational temperature for the ν_6 hot-band indicates that the vibrational relaxation from the ν_3-levels to the ν_6-levels is quite efficient. One can also say that the ν_6 level is overpopulated since the molecules are trapped in the vibrational state with the lowest energy. These results are in agreement with vibrational and rotational temperatures determined by Luijks *et al.*[11] in a Raman experiment.

Acknowledgements

We wish to thank:
— The National Institute of Public Health and Environmental Hygiene (RIVM) in Bilthoven for providing a tunable diode laser with detectors.
— The Dutch Foundation for fundamental Research on Matter (FOM) for financial support from the "Nederlandse Organisatie voor zuiver wetenschappelijk Onderzoek" (ZWO).
— Our technical staff, C. Sikkens, J. Holtkamp, F. van Rijn and L. Hendriks for their excellent support and contributions.
— And finally Prof. J. Reuss for his stimulating support and helpful comments.
— One of us (S. Stolte) acknowledges the CNRS for supporting his stay in the laboratory of Prof. J. P. Martin at Ecole Centrale des Arts et Manufactures, Chatenay Malbry. From this collaboration this work has benefitted greatly.

References

1. K. Burczyk, H. Bürger, A. Ruoff and B. Pinson, *J. Mol. Spec.* **77**, 109 (1979).
2. H. Bürger, K. Burczyk, H. Hollestein and M. Quack, *Mol. Phys.* **55**, 255 (1985).
3. A. Baldacci, A. Passerini and G. Ghersetti, *J. Mol. Spec.* **91**, 103 (1982).
4. L. C. Hoskins and C. L. Lee, *J. Chem. Phys.* **59**, 4932 (1973).
5. H. Burger, K. Burczyk, P. Schulz and A. Ruoff, *Spectr. Acta* **38A**, 627 (1982).
6. K. Burczyk, H. Bürger and P. Schulz, *Z. Anorg. Allg. Chem.* **474**, 74 (1981).
7. H. Jones, F. Kohler and D. Rudolph, *J. Mol. Spec.* **63**, 205 (1976).

7a. P. B. Davies and A. J. Morton-Jones, *J. Chem. Soc. Faraday Trans.* **81**, 1471 (1985).
7b. P. B. Davies and A. J. Morton-Jones, *Infrared Phys.* **25**, 215 (1985).
7c. P. B. Davies and A. J. Morton-Jones, *Appl. Phys.* **B42**, 35 (1987).

8. L. S. Rothman, A. Goldman, J. R. Gilis, R. H. Tipping, L. R. Brown, J. S. Margolis, A. G. Maki and L. D. Young, *Appl. Opt.* **20**, 1323 (1981).
9. G. Herzberg, *Molecular Spectra and Molecular Structure, vol. 2, Infrared and Raman Spectra of Polyatomic Molecules.* (Van Nostrand–Reinhold, New York, 1945.)
10. J. Sheridan and W. Gordy, *J. Chem. Phys.* **20**, 591 (1952).
11. G. Luijks, S. Stolte and J. Reuss, *Chem Phys. Lett.* **94**, 48 (1983).
12. J. M. Hartmann, M. Y. Perrin, J. Taine and L. Rosenmann, *J.Q.S.R.T.* **35**, 357 (1986).